Desalination and Water Treatment
www.deswater.com

doi: 10.5004/dwt.2022.28650

265 (2022) 1–17
July

Performance analysis of single slope solar still for different surface geometry of basin absorber

Kuber Nath Mishra[a], Anil Kr. Tiwari[a,*], G.N. Tiwari[b,c]

[a]*Department of Mechanical Engineering, National Institute of Technology Raipur, Chhattisgarh 492010, India, emails: aktiwari.mech@nitrr.ac.in (A.Kr. Tiwari), knmishra.phd2017.mech@nitrr.ac.in (K.N. Mishra)*
[b]*Jananayak Chandrashekhar University, Ballia, Uttar Pradesh 277301, India*
[c]*Bag Energy Research Society (BERS), 11B, Gyan Khand 4, Indirapuram, Ghaziabad Uttar Pradesh, 201014, India, email: gntiwari@ces.iitd.ernet.in (G.N. Tiwari)*

Received 29 January 2022; Accepted 10 June 2022

ABSTRACT

An investigation of performance for conventional single slope solar still with different surface geometry of basin absorber is reported in this article. Variation in surface geometry of the basin and its consequent effect on the hourly yield of the still is evaluated theoretically and compared with a conventional single slope solar still with unit basin absorber area as reference. An investigation of solar still with conventional (1 m^2), wire mesh large (1.004 m^2), wire mesh small (1.13 m^2), triangular cuts (1.29 m^2), semi cylindrical troughs (1.59 m^2), triangular corrugations (1.71 m^2), hemispherical depressions (1.79 m^2) and parabolic trough (1.80 m^2) as basin surface area value is investigated theoretically and wire mesh large, wire mesh small cases are also investigated experimentally. The mathematical model is utilized for arriving at respective heat transfer coefficient and hourly distillate yield values. The best suitable geometry of the still basin is reported based upon increment in heat transfer coefficients and hourly yield. The theoretical analysis is performed using MATLAB R2015a for climatic conditions of Raipur Chhattisgarh India for the month of June 2021 and the weather data is taken from the Indian Metrological Department (IMD), Pune, India. The cumulative hourly yield as obtained with respect to their respective surface area values is found to be 3.94, 4.31, 4.76, 5.68, 6.79, 7.35, 7.25 and 7.36 L corresponding to conventional, wire mesh large, wire mesh small, triangular cuts, semi cylindrical troughs, triangular corrugations, hemispherical depressions and parabolic trough respectively. The maximum deviation between the mathematically obtained and experimental values of hourly yield values is found to be 13.5% while the maximum deviation between the cumulative daily distillate yield is found to be 13.23% for wire mesh large.

Keywords: Solar stills; Basin surface geometry; Triangular cuts; Hemi spherical depressions; Parabolic trough

1. Introduction

Water is not only a source to fulfil all our biological needs but also a crucial sink for all the by-products of our daily activities. In near future its availability may also be limited by the degree to which it has been polluted over or underground. Since the major fraction of the water, just over half the total sustainable freshwater runoff does not make it back to the system, recycling and purification are the only paths remaining ahead to sustain human life on this planet. Water purification through reverse osmosis (RO) is currently the most popular technology to quench the thirst of the population in major parts of the globe. Being energy-intensive and polluting in nature, RO water purification needs a supplement and a replacement, if possible, with a more sustainable and eco-friendly technology that can be

* Corresponding author.

made available to all. One such promising technology on horizon is solar water distillation. It is simple, cost-effective, free to operate, highly scalable and has a low payback period compared to other purification technologies. The growing popularity of the solar technologies has resulted in a quest to minimise the only inherent drawback of the technology that is its inconsistent and unreliable nature of availability. Another major drawback holding back solar technology is technological inability to convert it to the useful form with a considerable efficiency. The scientist around the globe strive to improve the performance of the solar powered devices including solar stills. The still performance in terms of hourly, daily and annual distilled water yield depends upon numerous environmental factors and some key design parameters. Since the former cannot be controlled, the later has to be exploited in the best possible manner to extract maximum output from the prevailing environmental conditions. One of the means to improve the solar still yield is to augment the solar still basin surface geometry for improving heat transfer rates between the basin absorber and water. The present work has discussed a few of the methods to achieve higher basin surface area in order to achieve higher heat transfer rates and hence corresponding gain in hourly and daily yield.

The solar still design, thermal modelling and its applications are presented by Tiwari [1] and is the foundation for in-depth study of factors affecting solar still performance including the effect of surface area variation in solar devices upon their performance. In a fundamental study with respect to basin absorber material, Karthikeyan [2] has concluded that copper with its high value of thermal conductivity is more suitable than mild steel for the basin absorber fabrication. Fin addition to the solar still basin has a significant positive effect on the rate of basin water evaporation and can gain up to 53% in daily yield [3]. In a study by Modi and Jani [4] the increment in basin surface area by 23.78% has led to an average daily yield improvement of the order of 47.35% over the conventional double slope solar still. An experimental investigation on the performance of a pin finned wick absorber solar still by Alaian et al. [5] showed 23% productivity enhancement. Elshamy and El-Said [6] have presented a tubular solar still where the productivity is enhanced by 26.47% using semi-circular corrugated absorber against flat absorber geometry. Jani and Modi [7] have studied the effect of circular and square cross sectional hollow fins for variable water depth in the basin of a solar still and have found the circular fins to be superior than the square fins by a maximum of 54.22% in terms of daily desalinated water yield. Hafs et al. [8] have studied the rectangular, triangular and spherical corrugations in the solar still basin absorber and have hailed the use of rectangular corrugations over the other two configurations for domestic purposes. Kabeel et al. [9] have demonstrated for a reversed solar collector coupled with a hemispherical solar still that a v-corrugated basin surface results into a higher water surface area in contact with the basin. This leads to higher water temperature and consequently 68.82% higher yield compared to traditional flat basin hemispherical solar still. Darbari and Rashidi [10] have presented a theoretical model for yield improvement of a solar still by implementation of three different floating absorber geometries and have concluded the semi-circular shape as the best for achieving the highest yield value that is 65% higher than the conventional still. The model is validated using the experimental analysis by Agrawal and Rana [11] who have evaluated multiple V-shaped floating wicks for a single slope solar still. The increment in evaporative surface area by implementation of V-shaped wicks by 26% helped the solar still to achieve a gain in daily efficiencies by 56.62% and 47.75% in summer and winter respectively. In another attempt to augment solar still performance, Shalaby et al. [12] have investigated a solar still equipped with phase change material and V-type corrugations to enhance the distillate yield of a solar still and have obtained a 12% increment in daily yield.

The corrugated basin surface can also lead to a significant improvement in productivity up to 55.36% compared to a conventional solar still [13] and hence can be applied for solar still performance improvement. With fin integration an average of 40% improvement in yield can be obtained while the corrugated basin surface can result a 21% improvement in yield over a conventional still [14]. Apart from fins, sponges and wicks too can augment solar still productivity and can achieve productivity improvement of the order of 45.5%, 15.3% and 29.6%, respectively [15]. Fin height increment has a positive effect on the productivity while the fin thickness adversely affects the productivity. Also increasing the number of fins increases the shadow area and hence adversely affects the yield [16]. Despite the shadow effect, the fins have been found to improve yield by increasing the surface area of water in the basin and hence ensuring a quick start up with enhanced evaporation rates. The fins are also observed to reduce the bottom and side heat losses occurring in a conventional solar still [17]. The pin fin arrangement in the basin can result into a gain in productivity by 14.53% compared to a conventional still. The pin fins are found to boost the greenhouse effect in the solar still cavity thus boosting the rate of evaporation of basin water [18]. The total production rate of distilled water can be improved by 48.9% by means of a water coral fleece with stepped wire mesh absorber [19]. Addition of a PCM reservoir can also boost the solar still productivity when coupled with pin fins by 30% [20]. The use of blackened sponge in the basin absorber is found to yield good results during overcast and nocturnal periods for the solar still [21].

The above literature has widely highlighted the positive effect of surface area addition in solar still basin for performance appraisal. Hence the present work intends to present a detailed theoretical and experimental investigation into the effect of surface area gain by modification of basin surface geometry. The shadow effect for the fins into the basin is prominent at smaller solar altitude angles [22]. Hence this analysis is entirely presented for the month of June when the solar altitude angle is approximately highest for the year. A total of eight different cases with seven different modifications based upon their individual merit is investigated here for performance evaluation in terms of heat transfer coefficients occurring in the still and consequent hourly distilled water yield improvement. The basin modifications presented here are wire mesh large, wire mesh small, triangular cuts, semicylindrical troughs, triangular corrugations, hemispherical depressions and parabolic troughs.

2. System description

2.1. Theoretical analysis system description

A theoretical performance analysis of a single slope solar still with seven different basin surface geometries apart from the conventional plane surface geometry is presented in this work. Apart from flat basin of conventional solar still, the geometries under consideration for theoretical analysis here are wire mesh large (wire $mesh_L$), wire mesh small (wire $mesh_S$), triangular cuts, semicylindrical troughs (semi cyl. trough), triangular corrugations (tri corrugations), hemispherical depressions (hemi S. depressions) and parabolic troughs. The surface geometries are designed to contain 50 kg of basin water spread over a unit projected basin area and hence the heat transfer surfaces have been maximised for the given physical dimensions of the projected basin area and volume of the water in the basin. As the objective of the present work is to analyse the impact of basin surface geometry on the distilled water yield, the geometries chosen are simple (limited to regular polygons and shapes) for the purpose of simplifying the surface area and heat transfer calculations and more intricate geometries are proposed to be analysed further in future. Aluminium is chosen as the surface material placed over the galvanised iron (GI) sheet basin since it has a considerably higher thermal conductivity compared to the GI sheet used for the remaining parts of the still. The incident radiation passing through the gaps in case of perforations and wire mesh respectively is considered to be received by the GI sheet basin at the bottom. The performance characteristics of the modified still are compared with a conventional single slope solar still for June 1, 2021 at Raipur Chhattisgarh India.

2.2. Experimental setup fabrication and description

The experimental setup for single slope conventional solar still as presented here for the analysis is fabricated out of white PVC boards as outer and GI sheet as the basin and interior structure. The 4 mm thick float glass inclination cover is taken to be 23° with horizontal as per the geographical latitude of Raipur Chhattisgarh India. The conventional still basin absorber is made up of black painted plain GI sheet as the basin material without any modification to the geometry. The modified geometry solar still consists of the conventional solar still with placement of wire mesh arrangement as shown in Fig. 1.

The setup is operated for three consecutive days and the water lost in the form of distillate output is made up by adding equivalent quantity of water at the end of each day. This eliminates the need for a makeup water or feeding tank. The basin is fabricated to have unit projected area of the basin absorber upon which two of the chosen wire mesh geometries are placed on consecutive days for experimental observations. The still operation between 0700 and 1,800 h is only considered for the present analysis and the values recorded before and beyond this duration are neglected. The wire mesh is made up of aluminum and is framed in wooden supports for its placement in the basin. The hourly distillate yield observations are tabulated and recorded every hour for the stipulated duration. A detailed description of the wire mesh arrangement is presented in the succeeding section of this article. The physical dimensions of the conventional solar and other material details are provided in Table 1 and the wire mesh dimensions are described in Table 2. The two wire mesh configurations are shown in Fig. 2. The larger wire mesh is seen placed behind the smaller wire mesh in this figure.

Improving the solar radiation absorption at the basin absorber affects the solar still productivity significantly,

Table 1
Physical details for solar still setup fabrication

Criteria	Values, type
Outer structure construction material	PVC board, 17 mm thick
Basin material	GI Sheet
Glass thickness and type	4 mm float glass
Basin absorber surface finish	Matt black
Insulation	Polyurethane sheet, 41 mm thick
Mass of water in the basin	50 kg
Glass cover inclination angle	23°

Fig. 1. Conventional solar still setup and wire mesh placement in the basin.

Table 2
Chronological order of the theoretical and experimental analysis

Day	Basin heat transfer area (m^2)	Basin type	Analysis type	
June 1	1	Conventional plain basin absorber		
June 2	1.04	Wire mesh large (16 mm CTCD)	Experimental	
June 3	1.13	Wire mesh small (2 mm CTCD)		
June 1	1.29	Triangular cuts (equilateral, 0.01 m side length)		Theoretical
June 1	1.59	Semi cylindrical troughs (0.1268 m base diameter, 8 rows)		
June 1	1.71	Triangular corrugations (right angled, 0.08 m side length, 6 rows)	Theoretical	
June 1	1.79	Hemispherical depressions (0.19 m diameter, 28 depressions)		
June 1	1.80	Parabolic troughs (0.078 m depth, 0.33 m latus rectum, 3 rows		

Fig. 2. Large and small wire mesh (wire $mesh_L$ and wire $mesh_S$) for the basin.

since the otherwise loss of the solar radiation to the ambient can be more effectively utilized to heat the basin water [23]. Also, an increment in basin surface area leads to higher water temperature hence higher yield [13]. Thus, increase in basin surface area is a simple strategy to improve solar still distillate yield. In the present work, a few of the simple yet effective means of increasing the basin surface area have been investigated for their respective impact on the solar still performance.

3. Procedure adopted for the analysis

The procedure adopted for theoretical and experimental analysis is presented in the flow diagram in Fig. 3 and the sequence of cases considered for the present theoretical and experimental analysis is presented in Table 2.

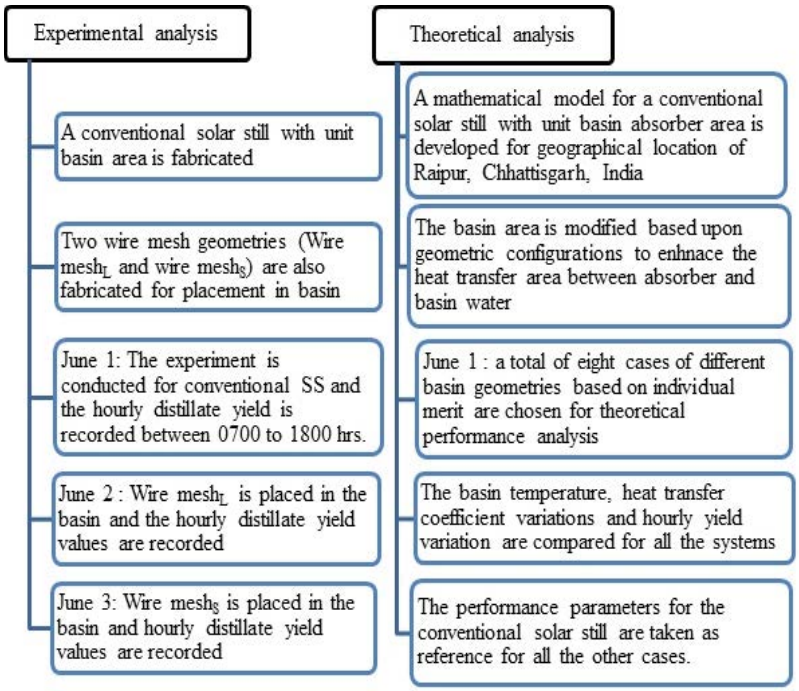

Fig. 3. Procedure adopted for experimental and theoretical analysis.

4. Instrumentation for experiments

Since the present work also compares the theoretical distillate yield for the wire mesh configurations with the experimentally obtained hourly distillate yield, the distillate output is measured by the weighing machine and measuring flask as shown in Fig. 4. The instrument error as obtained from the calibration data provided by the manufacturer is presented in Table 3.

The standard error "u" that can be arrived at by using standard error as provided by the calibration data for the above instruments can be calculated by the Eq. (1) [7]:

$$u = \frac{a}{\sqrt{3}} \tag{1}$$

where a is the instrument accuracy obtained from instrument calibration data.

5. Surface geometries chosen

The following geometrical configurations are proposed for the analysis:

5.1. Wire mesh (large and small)

A wire mesh can be a simple yet effective way to increase the basin surface area and hence improve the solar still yield. In the present manuscript, two wire mesh configurations have been implemented for the theoretical and experimental analysis. The configurations are named large and small based upon the wire diameter and the center-to-center distance (CTCD) between the consecutive wires. The large wire mesh (wire mesh$_L$) consists of a CTCD 0.016 m for a 0.001 m wire diameter. The surface area thus obtained is found to be 1.004 m^2. The calculations for net effective area for heat transfer for the wire mesh is presented in Appendix 1. The surface area so obtained for small wire mesh (wire meshs) is found to be 1.13 m^2 for a CTCD value of 0.002 m and wire diameter of 0.005 m.

Fig. 4. Weighing machine for measuring distillate yield.

5.2. Triangular cuts (equilateral)

Fig. 5 shows the triangular geometry in the basin for increasing the surface area of the absorber. For this configuration of basin surface, an optimum number of equilateral triangular sections are removed from the aluminium plate so as to maximise the absorber surface area as in the previous case of wire mesh. The equilateral triangle is said to be the geometric figure with maximum surface area for a given perimeter hence for a given side length, the area of a single equilateral triangle removed from the basin surface is maximum. The maximum area removal allowed is 50% of the basin surface here since utilising the entire basin surface for the triangular cuts makes the case same as wire mesh. Hence for the above reason and to maintain the structural integrity of the plate, only the half the plate surface is utilised for the triangular cuts. Thus, for a side length of 0.01 m a total of 11547 such triangles can be carved out of the plate to attain a maximum heat transfer area of 1.34 m^2.

Out of all the chosen dimensions for the triangle, an equilateral triangle with side length 0.01 m is chosen after analysing the effect of side length and number of triangles upon the total area of the basin absorber and increment in area. The increment in heat transfer surface is obtained in the form of increase in surfaces due to the perimeter of the triangles removed. The plate thickness considered here is 0.001 m and the surface area calculations are presented in Appendix 1.

5.3. Triangular corrugations

While the previous two basin absorber geometries are result of modifications in planar geometries, the one presented here is a three dimensional where the basin absorber surface is protruded in a right triangular projection above the basin. The geometry presented in this section and other forthcoming sections have been designed for a constant mass of 50 kg basin water. The configuration that can accommodate 50 kg water mass for the maximum surface area has been chosen as appropriate here. The right-angled triangle

Table 3
Instrument error

Instrument/sensor	Weighing scale Dr. trust (517) (kg)
Range	0–10
Accuracy (a)	±0.05
Standard error (u)	0.0288

[7] so obtained has a base side length equal to its vertical height and hence the increment in surfaces is a result of extended surfaces of vertical side and the slant side (hypotenuse). The longest side is assumed to face south so as to compensate for the solar radiation blockage due shadow caused by the projections. The rows are placed one base length apart so as to further reduce the effect of shadow on to the adjacent row. This implies that the 50% of the basin area is left unaltered in this case. The number of projected triangular rows that can accommodate a volume of 50 L (or 50 kg) of basin water within the solar still cavity as presented in Fig. 6 is found to be six for a base side length of 0.08 m resulting into a net gain of heat transfer area by a value of 71% hence the net effective heat transfer area available in this case is 1.71 m^2. The water is assumed to be filled exactly up to the vertex of the triangle. Here the maximum depth is found to be 0.08 m. The adverse effect of increase in water depth is negated by the fact that this is not a constant depth case as in conventional stills and at its minimum, depth of water can be said to be zero near the vertex of the projections. The surface area calculations for this case are presented in Appendix 1. Fig. 6 has a detailed description of the physical dimensions of the corrugations.

5.4. Hemispherical depressions

One of the major drawbacks with the surface area increment by means of projections above the basin is the shadow that is cast on to the adjacent surfaces. This may reduce the surface area available for effective interception of incident solar radiation. To overcome this, the projections may be oriented in the opposite direction and can be made into depressions. One such simple configuration is presented here. Since circles can only occupy 78.5% of a square area in which they are inscribed, to avoid overlapping of the circles, the depressions here are hemispherical with 78.5% of basin surface area occupied by the circles projected as the opening of the depressions. The maximum surface area obtained in this case is found to be 1.79 m^2 corresponding to a diameter/depth value of 0.19 m with 28 such depressions possible in the basin surface. In this case the basin water is assumed to be filled into the depressions. Extensive study of heat transfer phenomenon in such cases may be of great interest however the same is beyond the purview of the work presented in the current manuscript. The surface area calculation for this case is presented in Appendix 1. Fig. 7 represents the dimensions of the hemispherical depressions.

5.5. Semi cylindrical trough

Semi cylindrical troughs are another arrangement alternate to hemispherical depressions to increase the heat transfer surfaces in the present analysis. The troughs have an inherent advantage over the hemispherical depressions that they can accommodate same volume of water for a smaller value of maximum water depth. The maximum water depth in case of hemispherical depressions is found to be 0.19 m for 50 kg water mass while for the semi cylindrical troughs, the maximum water depth is found to be 0.12 m for a net gain of 59% of extended heat transfer surface. The reduction in maximum water depth is 36.8% compared to hemispherical depressions while the surface area is reduced by

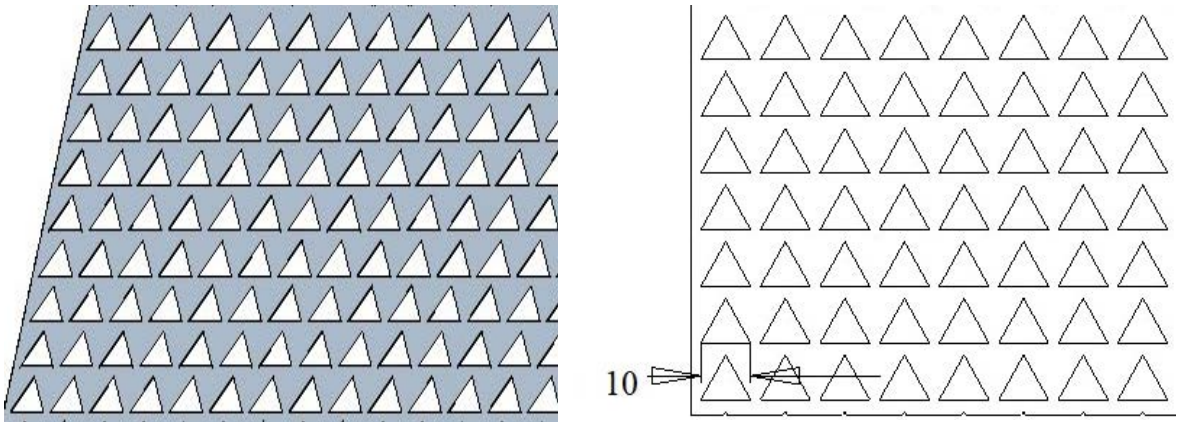

Fig. 5. Triangular cuts for extending the heat transfer area.

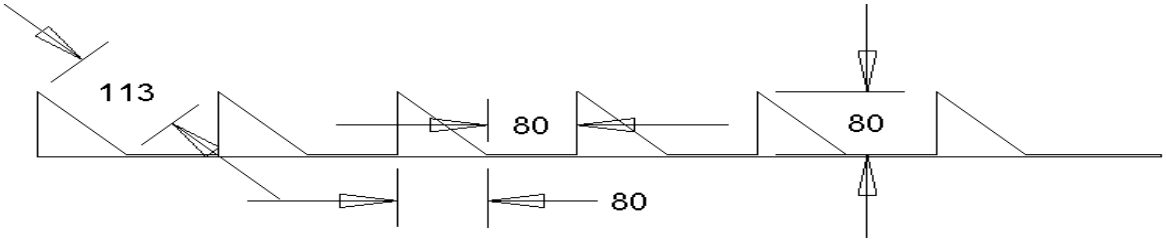

Fig. 6. Triangular corrugations for increemnt of heat transfer area.

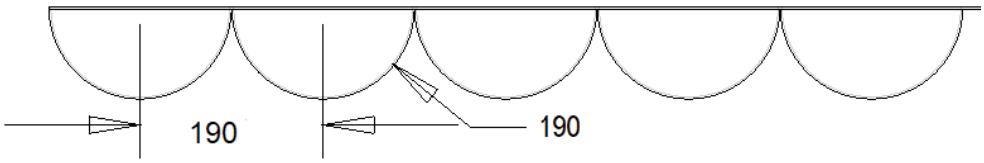

Fig. 7. Hemispherical depressions for heat transfer surface increment.

a value of 11.1%. The water is assumed to be filled up to the meeting edge of adjacent troughs. The surface area calculations are presented in Appendix 1 for the present case. Fig. 8 represents the semi cylindrical trough dimensions.

5.6. Parabolic trough

Parabolas can be extremely efficient in yielding a very high value of surface area for a given volume of the trough. The present analysis does not include the parabola characteristics from the focus and optical concentration point of view since they are painted black to maximize their absorptivity value and in the present analysis the parabola is considered to be only a method to achieve higher value of additional heat transfer surface. The semi cylindrical trough has a smaller value of maximum water depth, at cost of smaller value of surface area also. A parabola can offer the smaller water depth with higher value of surface area available for heat transfer. In the present case, three parabolic troughs with latus rectum value equal to 0.33 m that can accommodate 50 kg of water can offer a net surface area value of 1.80 m^2 for a maximum water depth value of 0.078 m. This is the highest value of the surface area among all the cases presented here. The detailed surface area calculation for this case is presented in Appendix 1. Fig. 9 represents the dimensions of the parabolic trough. The unit for the physical dimensions of the drawings in the manuscript are in mm:

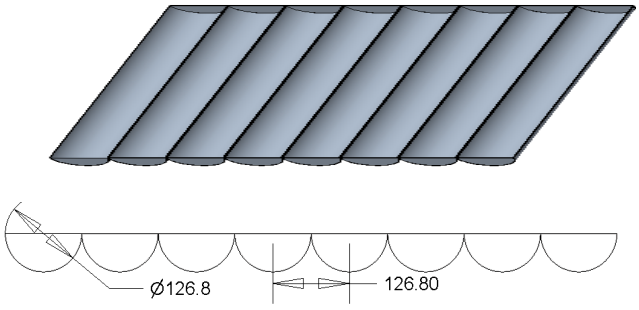

Fig. 8. Semi cylindrical troughs for heat transfer area gain.

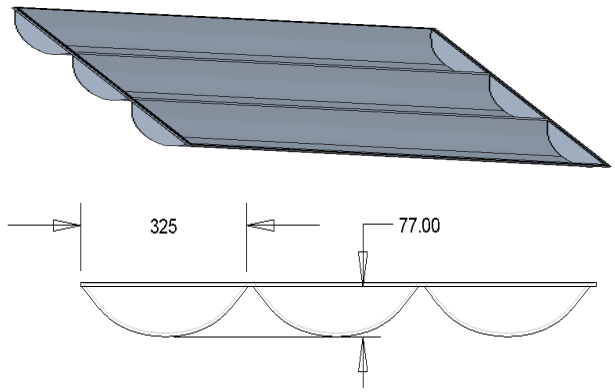

Fig. 9. Parabolic troughs for heat transfer surface extension.

6. Assumptions for mathematical modelling

For the purpose of simplification of the proposed analytical model, the following assumptions were made to arrive at the energy balance equation of the still components:

a. The temperature of the absorber is assumed to be same throughout the basin.
b. The heat capacity of absorber, glass cover and bottom insulation are neglected.
c. One dimensional heat conduction is considered for the present modeling.
d. The present modeling is based upon quasi-steady state.

7. Mathematical modelling

The mathematical modelling for the theoretical analysis is based upon the conventional solar still model developed by Mishra et al. [24]. All the equations for the conventional solar still are applicable for this case hence the thermal model only incorporates the extended basin surface area for heat transfer purposes. The design parameters for the solar still are provided in Table 4.

- Solar radiation fraction, absorbed by glass cover, water mass and basin liner are given as α'_g, α'_w and α'_b, respectively.

$$\alpha'_g = \left(1 - R_g\right)\alpha_g \tag{2}$$

$$\alpha'_w = \left(1 - \alpha_g\right)\left(1 - R_g\right)\left(1 - R_w\right)\alpha_w \tag{3}$$

$$\alpha'_b = \alpha_b\left(1 - R_g\right)\left(1 - \alpha_g\right)\left(1 - R_w\right)\left(1 - \alpha_w\right) \tag{4}$$

- Convective heat transfer coefficient, between glass surface and ambient.

Table 4
Design parameters

Parameter	Value
A_b, m²	1
h_w, W/m²	100
K_g, W/m K	0.816
L_g, m	0.004
K_i, W/m K	0.166
L_i, m	0.100
K_{abs}, W/m K	6
L_{abs}, m	0.002
L_i, m	0.100
C_w, J/kg K	4200
h_i, W/m²	2.8
α_{abs}	0.8
$U_{abs,amb}$, W/m² K	4.8
τ_g	0.95
α'_g	0.0095
α'_w	0.1787
α'_b	0.5861
M_w, kg	50
V, m/s	4.11

$$h_{cg} = 2.8 + 3.0\,V \tag{5}$$

- Temperature of sky.

$$T_{sky} = T_a - 6 \tag{6}$$

- Radiative heat transfer coefficient, from glass surface to sky.

$$h_{rg} = \frac{\varepsilon_g \sigma\left[\left(T_g + 273\right)^4 - \left(T_{sky} + 273\right)^4\right]}{\left(T_g - T_a\right)} \tag{7}$$

- Combined (convection + radiation) heat transfer coefficient, outer surface of glass.

$$h_{1g} = h_{cg} + h_{rg} \tag{8}$$

- Partial pressure at basin water surface.

$$P_w = e^{\left(25.317 - \frac{5{,}144}{T_w + 273}\right)} \tag{9}$$

- Partial pressure at glass inner surface.

$$P_g = e^{\left(25.317 - \frac{5{,}144}{T_w + 273}\right)} \tag{10}$$

- Convective heat transfer coefficient, from water surface to glass cover.

$$h_{cw} = 0.884\left[T_w - T_g + \frac{\left(P_w - P_g\right)\left(T_w + 273\right)}{268.9 \times 10^3 - P_w}\right]^{1/3} \tag{11}$$

- Evaporative heat transfer coefficient, from water surface to glass cover.

$$h_{ew} = 16.273 \times 10^{-3}\, h_{cw} \frac{P_w - P_g}{T_w - T_g} \tag{12}$$

- Effective emissivity between water surface and glass surface.

$$\varepsilon_{eff} = \left[\frac{1}{\varepsilon_g} + \frac{1}{\varepsilon_w} - 1\right]^{-1} \tag{13}$$

- Radiative heat transfer coefficient, from water surface to glass plate.

$$h_{rw} = \varepsilon_{eff}\sigma\left[\left(T_w + 273\right)^2 + \left(T_g + 273\right)^2\right] \times \left[T_w + T_g + 546\right] \tag{14}$$

- Total internal heat transfer coefficient.

$$h_{1w} = h_{cw} + h_{ew} + h_{rw} \tag{15}$$

- Combined (convective + radiative) heat transfer coefficient, bottom.

$$h_{crb} = 5.7 + 3.8\,V \tag{16}$$

- Heat transfer coefficient (conductive + convective + radiative) through bottom.

$$h_b = \left[\frac{L_i}{K_i} + \frac{1}{h_{crb}}\right]^{-1} \tag{17}$$

- Temperature of basin liner.

$$T_b = \frac{\alpha'_b I(t) + h_w T_w + h_b T_a}{h_w + h_b} \tag{18}$$

- Bottom heat loss coefficient.

$$U_b = \frac{h_w h_b}{h_w + h_b} \tag{19}$$

- Top heat loss coefficient, from water surface to ambient.

$$U_t = \frac{h_{1w} \times h_{1g}}{h_{1w} + h_{1g}} \tag{20}$$

- Overall heat loss coefficient.

$$U_L = U_b + U_t \tag{21}$$

- Value of factor.

$$a = \frac{U_L}{(\mathrm{MC})_w} \tag{22}$$

- Value of factor

$$(\alpha\tau)_{\mathrm{eff}} = \alpha'_b \frac{h_w}{h_w + h_b} + \alpha'_w + \alpha'_g \frac{h_{1w}}{h_{1w} + h_{1g}} \tag{23}$$

- Value of time factor.

$$\overline{f(t)} = \frac{(\alpha\tau)_{\mathrm{eff}} I(t) + U_L T_a}{(\mathrm{MC})_w} \tag{24}$$

- Average temperature of basin water.

$$T_{\mathrm{wavg}} = \frac{\overline{f(t)}}{a}\left[1 - \frac{\left(1 - e^{-a\Delta t}\right)}{a\Delta t}\right] + T_{w0}\frac{\left(1 - e^{-a\Delta t}\right)}{a\Delta t} \tag{25}$$

- Temperature of water after Δt time.

$$T_w = \frac{\overline{f(t)}}{a}\left[1 - e^{-a\Delta t}\right] + T_{w0}e^{-a\Delta t} \tag{26}$$

- Average temperature of glass plate cover.

$$T_{\mathrm{gavg}} = \frac{\alpha'_g I(t) + h_{1w}T_{\mathrm{wavg}} + h_{1g}T_a}{h_{1w} + h_{1g}} \tag{27}$$

- Temperature of glass plate cover after Δt time.

$$T_g = \frac{\alpha'_g I(t) + h_{1w}T_w + h_{1g}T_a}{h_{1w} + h_{1g}} \tag{28}$$

- Rate of evaporative heat loss.

$$q_{\mathrm{ew}} = h_{\mathrm{ew}}\left(T_{\mathrm{wavg}} - T_{\mathrm{gavg}}\right) \tag{29}$$

- Latent heat of water.

$$L = 2.4935 \times 10^6 \begin{bmatrix} 1 - 9.4779 \times 10^{-4} \times T_{\mathrm{wavg}} \\ +1.3132 \times 10^{-7} T_{\mathrm{wavg}}^2 \\ -4.7974 \times 10^{-9} T_{\mathrm{wavg}}^3 \end{bmatrix} \tag{30}$$

When $T_{\mathrm{wavg}} < 70°\mathrm{C}$;

- Latent heat of water.

$$L = 3.1615 \times 10^6 \left[1 - 7.6160 \times 10^{-4} T_{\mathrm{wavg}}\right] \tag{31}$$

When $T_{\mathrm{wavg}} < 70°\mathrm{C}$;

- Hourly distillate output.

$$m_{\mathrm{ew}} = \frac{h_{\mathrm{ew}}\left(T_{\mathrm{wavg}} - T_{\mathrm{gavg}}\right)}{L} \times 3{,}600 \tag{32}$$

The merit of this work lies in effective utilization of the basin area by addition of surfaces through geometric modifications. The area of the basin receiving the solar radiation remains constant while the effective area of heat transfer is higher due to the surface addition and modification.

8. Results and discussion

8.1. Solar radiation and ambient temperature variation

The incident solar radiation and ambient temperature data are taken from IMD Pune, India. Fig. 10 shows the solar radiation and ambient temperature variation for the days considered for the analysis. June 1 is chosen as the day for the conventional solar still performance analysis theoretically and experimentally. The hourly solar radiation

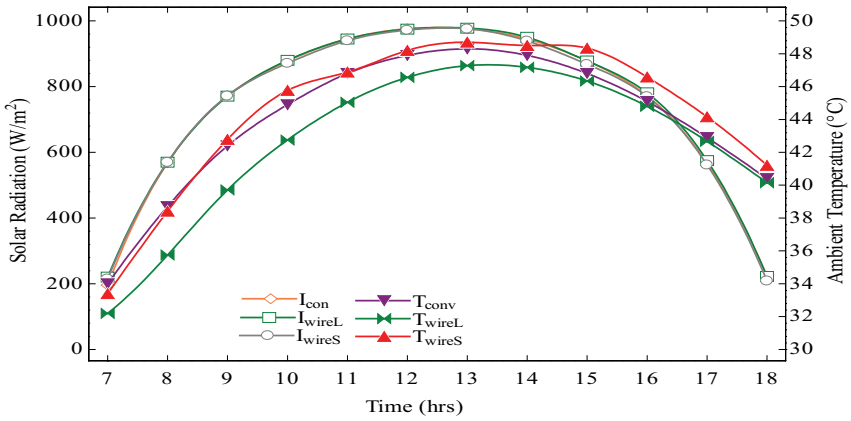

Fig. 10. Solar radiation and ambient temperature variation.

and ambient temperature variations for June 1 are applied for all the other cases of theoretical investigations while experimental and theoretical analysis for large wire mesh and small wire mesh are carried out for the radiation and ambient temperature data sets of the corresponding days of June 2 and 3 respectively. The peak solar radiation intensity for the three respective days is observed as 976, 978 and 976 W/m^2 at 1,300 h on all the days. The highest recorded ambient temperature is observed at the peak sunshine hours and are found to be 48.3, 47.2 and 48.7 at 1,300 h on all the three days as well.

8.2. Basin temperature variation with time

The basin absorber temperature is the most critical thermal parameter that determines all the other operational parameters of a conventional solar still operating under passive mode. Fig. 11 represents the basin temperature variation with respect to time for all the eight basin configurations. The basin water mass of 50 kg for all the cases is found to cause a shift in the peak basin temperature values to occur at 1,600 h instead of corresponding peak of the incident solar radiation observed at 1,300 h as shown in Fig. 10. The basin absorber temperature value trends for all the cases here are found to be in close proximity to each other for the early hours of 0700 to 0900 due to initial warm up time required for the basin water to achieve heat transfer towards glass surface. This is also evident from Figs. 12–15 where the difference between the heat transfer coefficient values is differentiable beyond 0900 h only. The role of basin surface area is observed to be significantly visible beyond 1,000 h when the setup has started generating differentiable distillate yield as per Fig. 16.

The highest basin temperature value of 95°C for the entire duration is obtained by the triangular corrugation basin at 1,600 h. Compared to the conventional solar still, this is an increment of 15.9%. The highest temperature achieved by hemispherical corrugations absorber plate in present case is 94.1°C that is 25.4% and 17.6% higher than the water temperature reported by Darbari and Rashidi [10] and Hafs et al. [8] for semicircular shaped tooth and rectangular fins respectively as means of enhancing the absorber surface area. This is only 0.7°C higher than the peak temperature value for the parabolic trough with highest value of heat

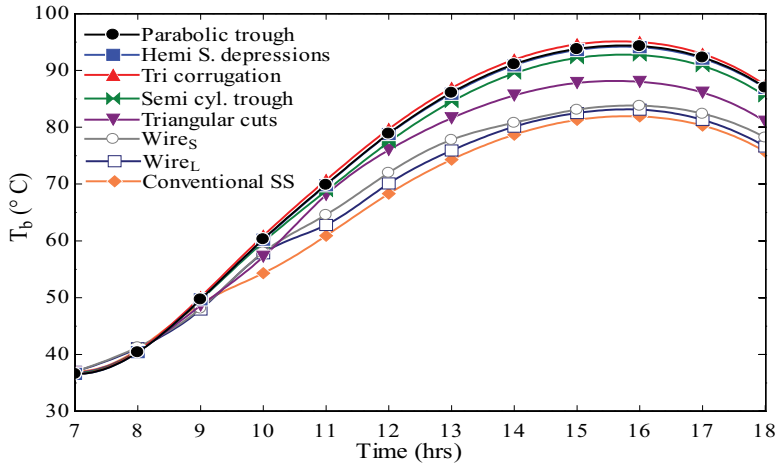

Fig. 11. Basin absorber temperature variation with time.

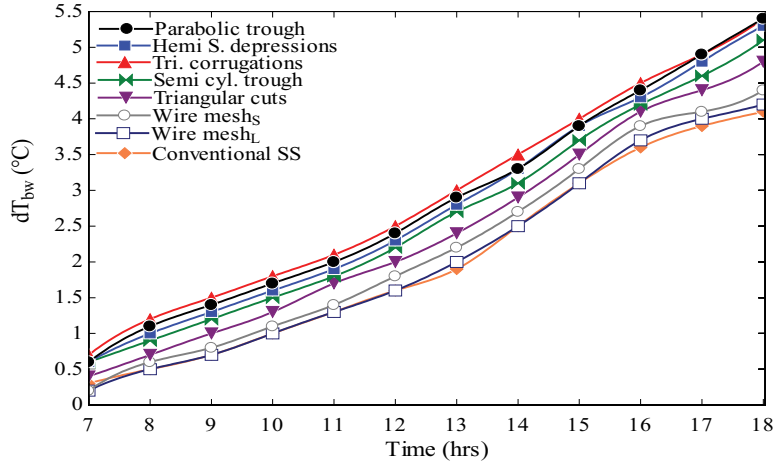

Fig. 12. Temperature difference variation for basin absorber and water.

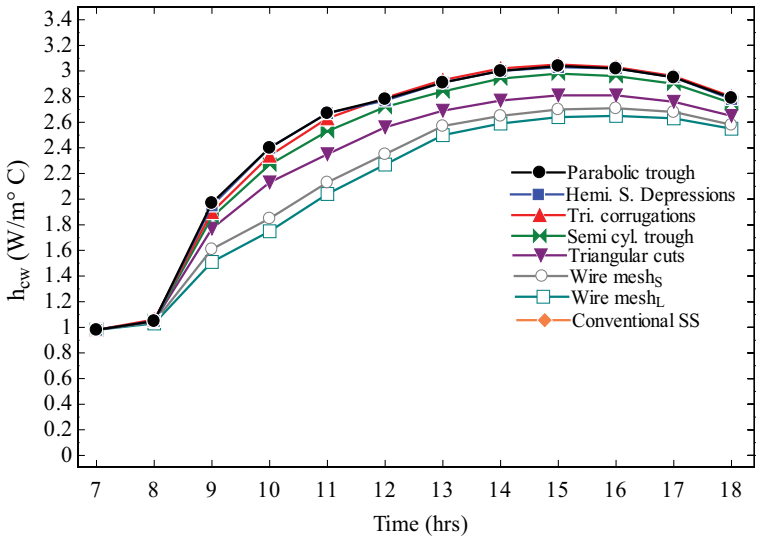

Fig. 13. Hourly variation of h_{cw} from water to glass cover.

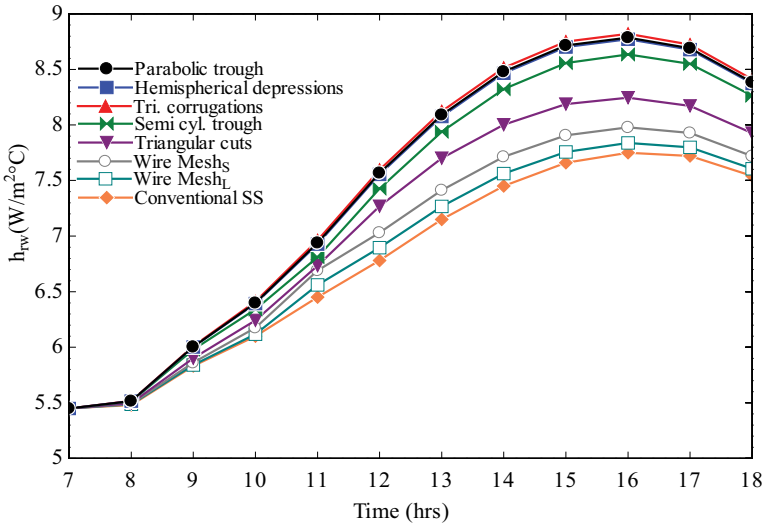

Fig. 14. Hourly variation of h_{rw} from water to glass cover.

transfer surface area. The peak basin temperature values for conventional, wire mesh large, wire mesh small, triangular cuts, semi cylindrical troughs, triangular corrugations, hemispherical depressions and parabolic trough are found to be 81.9°C, 83.1°C, 83.8°C, 88.0°C, 92.7°C, 95°C, 94.1°C and 94.3°C respectively, all occurring at 1,600 h. The basin temperature value depreciates after 1,600 h due to diminishing incident solar radiation as heat input and thermal loss in the form of distillate output.

8.3. Basin absorber and water temperature difference variation with respect to time

As reported by Tiwari [1] most of the incident solar radiation is received by the basin absorber after attenuation by the water mass. The attenuation is reported to be a function of water absorptivity and depth. Most of the heat as received by the absorber is convected back to the water while a small fraction is lost to the ambient in the form of bottom loss. As per Eq. (19), the bottom loss coefficient depends upon the heat transfer coefficient between still bottom and ambient, this in turn depends upon the temperature difference between basin absorber and ambient. From Eqs. (18) and (19) it can be inferred that the rising basin temperatures lead to a higher value of bottom losses and hence the trend as observed in Fig. 12 depicts that the temperature difference between water and basin ΔT_{bw} trend is corresponding to the basin temperature trend as in Fig. 11. The ΔT_{bw} values are observed to be increasing throughout the day for all the cases and the highest temperature difference between the basin absorber and water is found to occur at 1,800 h for all the cases under consideration. The peak ΔT_{bw} values for conventional, wire mesh large, wire mesh small, triangular cuts, semi cylindrical

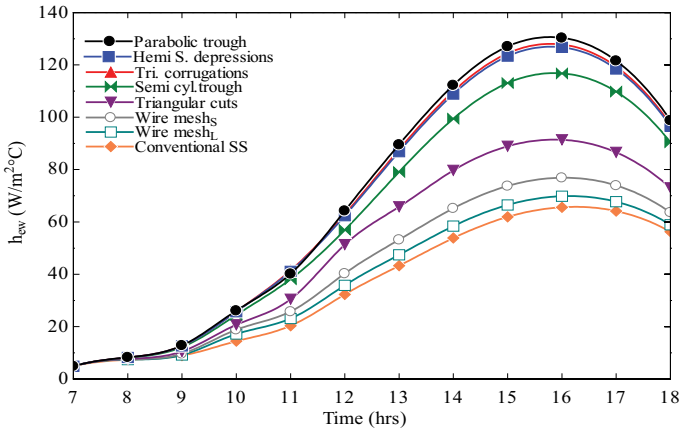

Fig. 15. Hourly variation of h_{ew} from water to glass cover.

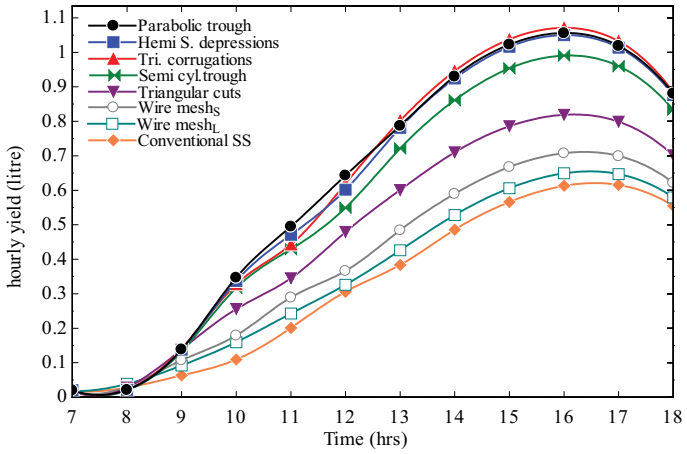

Fig. 16. Hourly variation of distillate yield.

troughs, triangular corrugations, hemispherical depressions and parabolic trough are found to be 4.1°C, 4.2°C, 4.4°C, 4.8°C, 5.1°C, 5.4°C, 5.3°C and 5.4°C respectively, all occurring at 1,800 h. This is due to the fact that the basin absorber temperatures are on the rise beyond the peak sunshine at 1,300 h up to 1,600 h while the ambient temperature has a comparatively sharp decline after 1,300 h. This leads to a higher bottom loss from the still for a larger temperature difference between the still basin and ambient.

It can be concluded from the above facts that the insulation considered in the conventional solar still may be insufficient for the geometries chosen here since the temperature range for the basin absorber is of the order of 95°C at its peak and the same is 12.4°C higher than the conventional solar still case for the same hour. The basin temperature profile for all the cases obtained here are similar to that reported in previous literature and in agreement with the same [24].

8.4. Variation of convective heat transfer coefficient (h_{cw}) from water to glass cover

The free convection inside the solar still cavity is the result of bouncy caused by the temperature difference between the basin water and the glass cover [1]. The heat transfer coefficient governing the transport of heat from water surface to glass is given by Eq. (12). It is evident from the equation that h_{cw} is directly proportional to the basin water temperature and hence rise in the basin water temperature leads to a corresponding rise in h_{cw} value. The h_{cw} trend for the eight different geometries under consideration here are a consequent result of the basin absorber temperature trend observed in Fig. 11.

The increment in heat transfer area by means of extended surfaces by all the means reported here reduces the preheating time proportional to the temperature gained by the water [6]. This is evident from the sharp rise in convective heat transfer coefficient value immediately after 0800 h. The additional surfaces lead to higher heat transfer values between the basin and absorber.

The lowest h_{cw} trend can be seen for the conventional solar still with lowest 1 m^2 of heat transfer surface while the highest trend can be seen for parabolic trough with a net surface area value of 1.80 m^2. This is closely followed by the trend for hemispherical depressions with a surface area value of 1.79 m^2. The peak h_{cw} values for all the cases are found to occur at 1,500 h since the maximum basin water temperature is also achieved between 1,500

to 1,600 h. The values are observed to decline after 1500 h due to decline in heat input value form solar radiation. The maximum h_{cw} value for conventional, wire mesh large, wire mesh small, Triangular cuts, semi cylindrical troughs, triangular corrugations, hemispherical depressions and parabolic trough are found to be 2.60, 2.64, 2.7, 2.81, 2.98, 3.03, 3.04, and 3.05 W/m°C respectively, all occurring at 1,500 h. The highest value of h_{cw} for parabolic trough with highest heat transfer area value of 1.80 m^2 is found to be 16.90% higher than the conventional solar still with unit area of basin surface. Modi and Jani [4] have claimed the benefits of the extended surfaces as a way to not only increase heat transfer values but also to absorb higher incident solar radiation. The proposed work presents the role of extended surfaces as a means of improving the heat transfer characteristics only while the area receiving the incident radiation is considered to be 1 m^2 for all the cases.

8.5. Variation of radiative heat transfer coefficient (h_{rw}) from water surface to glass

Fig. 10 is an illustration of variation of radiative heat transfer coefficient (h_{rw}) from water surface to glass cover for all the cases ranging from conventional solar still with unit basin area up to parabolic trough with highest basin area. The general trend for this parameter is observed to exhibit similar trend as that obtained for h_{cw} since the heat radiated from a mass depends upon the temperature of the body, the h_{rw} for all the cases reported here are found to occur at 1,600 h since the peak for basin water temperature is also found to occur at the same time. The peak h_{rw} value for conventional, wire mesh large, wire mesh small, Triangular cuts, semi cylindrical troughs, triangular corrugations, hemispherical depressions and parabolic trough are found to be 7.75, 7.83, 7.97, 8.24, 8.63, 8.81, 8.77 and 8.78 W/m°C respectively, all occurring at 1,600 h. The highest value of h_{rw} for parabolic trough with highest heat transfer area value of 1.80 m^2 is found to be 13.41% higher than the conventional solar still.

8.6. Variation of evaporative heat transfer coefficient (h_{ew}) from water surface to glass

The most dominant and decisive heat transfer coefficient in a solar still is the evaporative heat transfer coefficient (h_{ew}) since this decides the amount of heat expenditure in evaporation of basin water and hence directly decides the final yield output from the solar still. The basin surface augmentations as reported here are all found to exhibit increase in heat transfer coefficient values in proportion to basin and water temperature which in turn is proportionate to the basin surface area available for heat transfer from basin to water. The lowest trend as can be observed from Fig. 11, is yet again obtained for the conventional solar still with smallest basin surface area while the highest trend can be observed for the parabolic trough. The h_{ew} values for all the cases have peaks at 1,600 h beyond which the values tend to decline due to drop in basin water temperature as a result of reduction in incident solar radiation value. The peak h_{ew} value for conventional, wire mesh large, wire mesh small, triangular cuts, semi cylindrical troughs, triangular corrugations, hemispherical depressions and parabolic trough are found to be 65.60, 69.82, 76.86, 91.38, 116.75, 127.78, 126.71 and 130.34 W/m°C respectively, all occurring at 1600 h. The highest value of h_{ew} for parabolic trough with highest heat transfer area value of 1.80 m^2 is found to be 98.68% higher than the conventional solar still. This indicates an almost double heat transfer rate for an 80% basin surface area gain by means of surface additions. The improvement in h_{ew} value corresponding to increase in surface area as reported in the present work is in accordance with the work previously reported by Modi and Jani [4]. The average temperature difference between water and glass cover that determines the value of h_{ew} as per Eqs. (11) and (12) is shown to increase with an increase in basin surface area and is also observed by Modi and Jani [4] and Hafs et al. [8].

8.7. Hourly yield variation (m_{ew})

The hourly yield of a solar still is a direct representation of the temperature difference between the basin water and the glass cover. The highest possible basin water temperature coupled with lowest corresponding glass cover temperature is the most desirable condition for a solar still. Since this leads to higher rates of evaporation and condensation of water. Thus, the hourly yield trend as depicted in Fig. 16 follows the component temperature trend specifically the basin absorber temperature that further corresponds to the heat transfer coefficients trends as presented. Here in Fig. 16, a similar trend in correspondence with basin temperature and heat transfer coefficient trends can be observed where the hourly yield value peaks at 1,600 h after steady increment form 800 h, beyond 1,600 h the values start to diminish gradually due to lack of heat input in the form of incident solar radiation. It has been observed that at lower basin water mass, the distillate yield peak is in strict correspondence with the peak in solar intensity radiation however with increase in mass, this peak is found to shift towards the later part of the day due to thermal inertia effect.

The peak hourly yield values occurring at 1,600 h and cumulative yield for the day between 0700 to 1,800 h corresponding to conventional, wire mesh large, wire mesh small, triangular cuts, semi cylindrical troughs, triangular corrugations, hemispherical depressions and parabolic trough are found to be 0.61, 0.65, 0.71, 0.82, 0.99, 1.07, 1.05, 1.06 and 3.94, 4.31, 4.76, 5.68, 6.79, 7.35,7.25 and 7.36 L respectively. The parabolic trough with highest value of heat transfer surface is found to obtain a 72.3% higher peak yield for an 80% higher surface area at 1,600 h compared to conventional solar still. The cumulative yield for the parabolic trough is found to be 86.7% higher than the conventional solar still. The quick starting time and higher relative basin temperature for the cases with extended basin absorber surface area is the cause for significantly higher distillate yield beyond 900 h and is this is validated by the works earlier reported by Agrawal and Rana [11], Hafs et al. [8] and Jani and Modi [7].

9. Comparison of hourly and total daily distillate yield

9.1. Experimental hourly yield comparison with theoretical hourly distillate yield

The two wire mesh sizes as shown in Fig. 2 are used for experimental observations for 2 days starting June 2, 2021 while the very first day of the experimentation is chosen as June 1 for the conventional solar still with unit basin surface area followed by the day with 16 mm wire mesh (centre to centre distance) on June 2. On June 3, the smaller 0.5 mm diameter and 2 mm (CTCD) wire mesh is chosen for experimentation. Table 1 presents the order in which the experiments and the theoretical analysis is carried out in the present work.

Fig. 17 shows the hourly yield variation for conventional, large wire mesh and small wire mesh basin absorber surfaces between 700 to 1,800 h for June 1, 2 and 3 respectively. The peak distillate yield values for the three cases obtained experimentally and theoretically are obtained at 1,600 h for each day. The corresponding theoretical hourly yield for conventional solar still, wire mesh large and wire mesh small are found to be 0.61, 0.65 and 0.66 L respectively, while the yield obtained experimentally for the same duration is found to be 0.59, 0.64 and 0.60 L respectively. The maximum deviation from the theoretically predicted hourly yield values is found to occur at 1,200 h for conventional solar still for a 13.5% smaller experimental yield value, at 1,800 h for wire $mesh_L$ for 8.5% maximum deviation value and 1,500 h for wire $mesh_S$ for corresponding theoretical yield values of 0.30, 0.60 and 0.58 L respectively. The deviations in hourly yield values are caused by environmental factors like wind velocity and ambient temperature variations.

9.2. Cumulative yield comparison

Fig. 18 represents the cumulative distillate yield for all the eight cases considered for theoretical analysis and the three cases for experimental analysis. As evident from Figs. 12 and 15, the hourly distillate yield strongly depends upon the basin absorber surface area and heat transfer rate between basin absorber and water which in turn is decisive in determining the rate of evaporation and condensation of water at the glass surface.

The theoretical cumulative daily yield for the conventional solar still (1 m^2), wire mesh large (1.004 m^2), wire mesh small (1.13 m^2), triangular cuts (1.29 m^2), semi cylindrical troughs (1.59 m^2), triangular corrugations (1.71 m^2), hemispherical depressions (1.79 m^2) and parabolic trough (1.80 m^2) are 3.94, 4.31, 4.76, 5.68, 6.79, 7.35,7.25 and 7.36 L/m^2/d, respectively. The percentage gain in daily cumulative yield for the above cases compared with conventional solar still is found to be 9.4, 20.8, 44.2, 72.3, 86.5, 84.0 and 86.8%, respectively. The present cumulative yield values for triangular cuts with an improvement of 44.2% over conventional still are in accordance with a 47.35% and 43.86% daily yield improvement reported by Modi and Jani [4] and Jani and Modi [7] for absorber surface area increment of 23.78% by means of hollow fins and circular fins over rectangular fins respectively.

The experimental cumulative yield is observed to exhibit similar trend as the theoretically obtained values

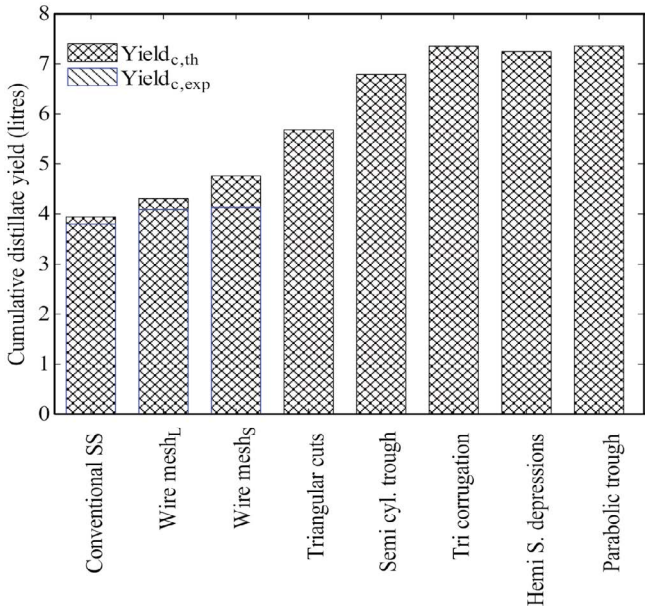

Fig. 18. Comparison of theoretical cumulative distillate yield for all the cases.

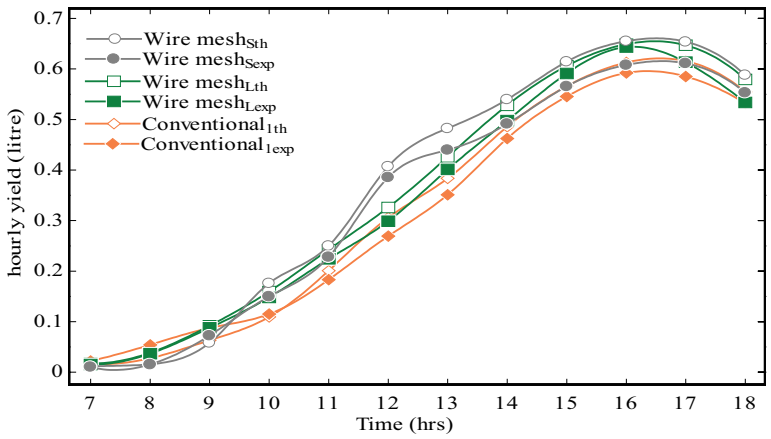

Fig. 17. Comparison of theoretical and experimental hourly yield.

however a deviation from the theoretically predicted values as a result of internal and external uncertainties leads to comparatively smaller values of cumulative yield foe all the three cases and hence an error or deviation of the magnitude of 13.23% (maximum) is obtained in the present analysis. The maximum deviation from the theoretically predicted cumulative yield for the experimentally obtained yield is found to be 13.23% for wire mesh$_S$ and 5.1%, 3.5% for wire mesh$_L$ and conventional solar still respectively. The comparatively higher basin absorber temperature as shown in Fig. 12 resulting into higher bottom heat losses for wire mesh$_S$ with respect to conventional solar still and wire mesh$_L$ throughout the day can be attributed for this phenomenon.

10. Conclusions

- The basin surface area augmentation for improving the heat transfer coefficient values in a solar still is an effective means of improving hourly yield.
- The surface area increment has a direct positive effect on the basin water temperature and hence the heat transfer coefficients.
- The bottom insulation has a vital role in solar still performance and an insufficient insulation can cause a drop in absorber temperature by 5.4°C.
- The maximum h_{cw}, h_{rw} and h_{ew} value for parabolic trough with highest heat transfer area value of 1.80 m^2 is found to be 16.90%, 13.41% and 98.68% higher than the conventional solar still with unit area of basin absorber surface.
- The parabolic trough with highest value of heat transfer surface is found to obtain a 72.3% higher peak yield and 86.7% higher cumulative yield for an 80% higher surface compared to a conventional solar still.
- The maximum deviation between the experimental and theoretical hourly yield and cumulative daily yield values for conventional, wire mesh large and wire mesh small case is found to be 13.5%, 8.6% and 8.5% and 13.23%, 5.1% and 3.5% respectively. With a maximum deviation value of 13.5% and 13.23% the present theoretical model can be said to be in good agreement with the experimental values obtained.

Symbols

R_g	—	Reflectivity of glass plate cover, fraction
α_g	—	Absorptivity of glass plate cover, fraction
α'_g	—	Solar radiation fraction, absorbed by glass cover, fraction
R_w	—	Reflectivity of water surface, fraction
α_w	—	Absorptivity of water, fraction
α'_w	—	Solar radiation fraction, absorbed by water mass, fraction
α_b	—	Absorptivity of basin liner material, fraction
α'_b	—	Solar radiation fraction, absorbed by basin liner, fraction
V	—	Velocity of wind over glass surface, m/s
h_{cg}	—	Convective heat transfer coefficient between glass and ambient, W/m^2°C
T_a	—	Ambient temperature, °C
T_{sky}	—	Sky temperature, °C
ε_g	—	Emissivity of glass plate cover, fraction
σ	—	Stiffen Boltzman constant = 5.67 × 10^{-8} W/m^2 K^4
T_g	—	Temperature of glass plate, °C
T_{gavg}	—	Average temperature of glass plate cover, °C
h_{rg}	—	Radiative heat transfer coefficient, from glass to sky, W/m^2°C
h_{1g}	—	Combined (convection + radiation) heat transfer coefficient from outer surface of glass, W/m^2°C
T_w	—	Temperature of water in basin, °C
T_{wavg}	—	Average temperature of basin water, °C
P_w	—	Partial pressure at water surface, N/m^2
P_g	—	Partial pressure at glass inner surface, N/m^2
h_{ew}	—	Convective heat transfer coefficient, water surface to glass cover, W/m^2°C
h_{ew}	—	Evaporative heat transfer coefficient, water surface to glass cover, W/m^2°C
ε_w	—	Emissivity of water surface, fraction
ε_{eff}	—	Effective emissivity between water surface and glass surface
h_{rw}	—	Radiative heat transfer coefficient, from water surface to glass plate, W/m^2°C
h_{1w}	—	Total internal heat transfer coefficient, W/m^2°C
$I(t)$	—	Incident total solar radiation, W/m^2
h_w	—	Convective heat transfer coefficient, between basin and water, W/m^2°C
h_{crb}	—	Combined heat transfer coefficient from bottom, W/m^2°C
L_i	—	Thickness of insulation, m
K_i	—	Thermal conductivity of insulation, W/m^2°C
h_b	—	Heat transfer coefficient, from bottom, W/m^2°C
T_b	—	Temperature of basin absorber, °C
ΔT_{bw}	—	Temperature difference between basin absorber and water, °C
U_b	—	Bottom heat loss coefficient, from water to ambient through basin, W/m^2°C
U_t	—	Top heat loss coefficient, from water surface to ambient, W/m^2°C
U_L	—	Overall heat loss coefficient, W/m^2°C
$(MC)_w$	—	Product of mass of water in basin (kg) and specific heat of water, J/kg°C
a	—	Factor
$(\alpha\tau)_{eff}$	—	Factor
$f(t)$	—	Factor
Δt	—	Time, s
T_{w0}	—	Temperature of water at t = 0, °C
q_{ew}	—	Rate of evaporative heat loss, W/m^2
L	—	Latent heat of vaporization of water, J/kg
m_{ew}	—	Hourly distillate output, kg/m^2 h

References

[1] G.N. Tiwari, Solar Energy: Fundamentals, Design, Modelling and Applications, Narosa Publishing House, India, 2016.

[2] S. Karthikeyan, Comparative study on passive solar still with copper and mild steel absorber basin trays, Mater. Today: Proc., 45 (2021) 7926–7929.

[3] V. Velmurugan, C.K. Deenadayalan, H. Vinod, K. Srithar, Desalination of effluent using fin type solar still, Energy, 33 (2008) 1719–1727.

[4] K. Modi, H. Jani, Experimental and theoretical assessment of dual-slope single-basin solar still with the circular cross-sectional hollow-fins, Cleaner Eng. Technol., 4 (2021) 100231, doi: 10.1016/j.clet.2021.100231.

[5] W.M. Alaian, E.A. Elnegiry, A.M. Hamed, Experimental investigation on the performance of solar still augmented with pin-finned wick, Desalination, 379 (2016) 10–15.

[6] S.M. Elshamy, E.M.S. El-Said, Comparative study based on thermal, exergetic and economic analyses of a tubular solar still with semi-circular corrugated absorber, J. Cleaner Prod., 195 (2018) 328–339.

[7] H.K. Jani, K.V. Modi, Experimental performance evaluation of single basin dual slope solar still with circular and square cross-sectional hollow fins, Solar Energy, 179 (2019) 186–194.

[8] H. Hafs, M. Asbik, H. Boushaba, A. Koukouch, A. Zaaoumi, A. Bah, O. Ansari, Numerical simulation of the performance of passive and active solar still with corrugated absorber surface as heat storage medium for sustainable solar desalination technology, Groundwater Sustainable Dev., 14 (2021) 100610, doi: 10.1016/j.gsd.2021.100610.

[9] A.E. Kabeel, M.E.H. Attia, M.E. Zayed, M. Abdelgaied, A.S. Abdullah, W.M. El-Maghlany, Performance enhancement of a v-corrugated basin hemispherical solar distiller combined with reversed solar collector: an experimental approach, Renewable Energy, 190 (2022) 330–337.

[10] B. Darbari, S. Rashidi, Performance analysis for single slope solar still enhanced with multi-shaped floating porous absorber, Sustainable Energy Technol. Assess., 50 (2022) 101854, doi: 10.1016/j.seta.2021.101854.

[11] A. Agrawal, R.S. Rana, Theoretical and experimental performance evaluation of single-slope single-basin solar still with multiple V-shaped floating wicks, Heliyon, 5 (2019) e01525, doi: 10.1016/j.heliyon.2019.e01525.

[12] S.M. Shalaby, E. El-Bialy, A.A. El-Sebaii, An experimental investigation of a v-corrugated absorber single-basin solar still using PCM, Desalination, 398 (2016) 247–255.

[13] Z.M. Omara, A.E. Kabeel, A.S. Abdullah, F.A. Essa, Experimental investigation of corrugated absorber solar still with wick and reflectors, Desalination, 381 (2016) 111–116.

[14] Z.M. Omara, M.H. Hamed, A.E. Kabeel, Performance of finned and corrugated absorbers solar stills under Egyptian conditions, Desalination, 277 (2011) 281–287.

[15] V. Velmurugan, M. Gopalakrishnan, R. Raghu, K. Srithar, Single basin solar still with fin for enhancing productivity, Energy Convers. Manage., 49 (2008) 2602–2608.

[16] A.A. El-Sebaii, M.R.I. Ramadan, S. Aboul-Enein, M. El-Naggar, Effect of fin configuration parameters on single basin solar still performance, Desalination, 365 (2015) 15–24.

[17] H. Panchal, I. Mohan, Various methods applied to solar still for enhancement of distillate output, Desalination, 415 (2017) 76–89.

[18] K. Rabhi, R. Nciri, F. Nasri, C. Ali, H.B. Bacha, Experimental performance analysis of a modified single-basin single-slope solar still with pin fins absorber and condenser, Desalination, 416 (2017) 86–93.

[19] R. Samuel Hansen, C. Surya Narayanan, K. Kalidasa Murugavel, Performance analysis on inclined solar still with different new wick materials and wire mesh, Desalination, 358 (2015) 1–8.

[20] J. Kateshia, V.J. Lakhera, Analysis of solar still integrated with phase change material and pin fins as absorbing material, J. Energy Storage, 35 (2021) 102292, doi: 10.1016/j.est.2021.102292.

[21] M.H. Sellami, T. Belkis, M.L. Aliouar, S.D. Meddour, H. Bouguettaia, K. Loudiyi, Improvement of solar still performance by covering absorber with blackened layers of sponge, Groundwater Sustainable Dev., 5 (2017) 111–117.

[22] K.M. Bataineh, M.A. Abbas, Performance analysis of solar still integrated with internal reflectors and fins, Sol. Energy, 205 (2020) 22–36.

[23] R.P.N. Ayuthaya, P. Namprakai, W. Ampun, The thermal performance of an ethanol solar still with fin plate to increase productivity, Renewable Energy, 54 (2013) 227–234.

[24] K.N. Mishra, Md. Meraj, A.K. Tiwari, G.N. Tiwari, Performance evaluation of PVT-CPC integrated solar still under natural circulation, Desal. Water Treat., 156 (2019) 117–125.

Appendix 1

A1. Case of wire mesh (large and small)

No. of wires in one way = $\frac{\text{Length of wire}}{\text{Center to Center Distance}}$

Surface area of one wire with junction point = $\frac{22}{7}\times\frac{\text{Diameter of wire}}{2}\times\text{Length of wire}$

Surface area of one wire without junction point =

(Length of wire – No. of wires in one way × diameter of wire) × $\frac{22}{7}\times\frac{\text{diameter of wire}}{2}$

Total exposed surface area of wire =

Surface area of one wire with junction point × No. of wires in one way + Surface area of one wire without junction point × No. of wires in one way

Projected area of one wire with junction point = diameter of wire × length of wire

Projected area of one wire without junction point = (Length of wire – No. of wires in one way × diameter of wire) × diameter of wire

Total projected area of wire in basin = Projected area of one wire with junction point × No. of wires in one way + Projected area of one wire without junction point × No. of wires in one way

Uncovered area of basin = Area of basin – Total projected area of wire in basin

Total exposed area of basin including wire = Uncovered area of basin + Total exposed surface area of wire

Shaded area due to one wire =

$A_{sh} = H_f \times l_{sh} \times \sin l + H_f \times l_{sh} \times \cos l - l_{sh}^2 \times \sin l \times \cos l$,

where H_f = Height of wire = Diameter of wire

l_{sh} = Length of shadow due to wire

l = latitude angle of location

Shaded area due to n wire in one way = Shaded area due to one wire × No. of wires in one way

Net effective area for heat transfer = Total exposed area of basin including wire – Shaded area due to n wire in one way

A2. Case of triangular cuts

Single triangle area = $\sqrt{\frac{3}{4}}\times\text{side}^2$

No. of triangles possible = $\frac{\text{Area of basin}}{\text{Area of one triangle}}$

No. of triangles at 50% plate area = $\frac{\text{No of triangle}}{2}$

Perimeter of all triangles = Triangle side length × 3 × No. of triangles at 50% plate area

Area addition by perimeter = Perimeter of all triangles × thickness of triangle

Total heat transfer exposed area = Area of basin + Area addition by perimeter

Net effective area for heat transfer = Area of basin + Area addition by perimeter

A3. Case of semi-cylinder

Length of semicylinder = width of basin

Area of one semicylinder = $\frac{22}{7}\times\frac{\text{diameter of cylinder}}{2}\times$ length of semicylinder

Vertical projected area of one semicylinder = Diameter of cylinder × Length of semicylinder

No. of cylinders in total basin area = $\frac{1}{\text{diameter of semicylinder}}$

Total surface area of semicylinder = No. of cylinder in total basin area × Area of one semicylinder

Height of semicylinder = Diameter of semicylinder

A4. Case of triangular corrugations

Width of triangle = $\frac{\text{Width of basin}}{}$

Hypotenuse length = $\sqrt{\text{side}^2+\text{side}^2}$

Height of triangle = Side of triangle

Exposed surface area of one triangle = (Hypotenuse length + height of triangle) × Width of triangle

No. of triangles in 50% area = $\frac{\text{50\% length of basin}}{\text{base side length}}$

Vertical projected surface area of one triangle = Base side length × Width of triangle

Exposed surface area of all triangles = No. of triangles in 50% area × Exposed surface area of one triangle

Total exposed surface area of basin including triangle = Exposed surface area of all triangle + 50% area of basin

A5. Case of hemispherical depressions

Surface area of one hemisphere = $2\times\frac{22}{7}\times\left(\frac{D}{2}\right)^2$

Projected circle area of one hemisphere = $\frac{\text{Surface area of one hemisphere}}{2}$

No. of circles possible in total area of basin = $\frac{1}{\text{area of square containg the circle}}$

Area occupied by one circle in one square = 78.5%

Total surface area of all hemisphere = No. of circles in total area of basin × Surface area of one hemisphere

Projected surface area of all circles = No. of circles in total area of basin × Projected circle area of one hemisphere

Net exposed surface area = Surface area of one hemisphere × No. of circles + (1 – 0.785)

A6. Case of parabolic troughs

It is assumed that focus of parabola lies at plane of basin

Hence, depth of parabola = Focus of parabola

Value of $x = \sqrt{y}$

Half perimeter of parabola = $\int_0^{\text{depth of parabola}}\sqrt{1+4x^2}\,dx$

Full perimeter of parabola = 2 × Half perimeter of parabola

Length of parabola = Length of basin = 1 m

Area of one parabola = Length of parabola × Full perimeter of parabola

Length of latus rectum = $4a$ in equation ($y^2 = 4ax$)

No. of parabolic troughs in total area of basin = $\frac{1}{\text{length of latus rectum}}$

Vertical projected area of one parabola = Length of latus rectum × Width of basin

Surface area of all troughs = No. of troughs in total area of basin × Surface area of one parabola

Projected area of all troughs = No. of parabola in total area of basin × Vertical projected area of one trough

Increase in area due to troughs = Area of all troughs – Projected area of all troughs